Modal analysis method to describe weak nonlinear effects in metamaterials

Y. Zeng and D. A. R. Dalvit
Theoretical Division, MS B213, Los Alamos National Laboratory, Los Alamos, New Mexico 87545, USA

J. O'Hara
Electrical and Computer Engineering, Oklahoma State University, Stillwater, Oklahoma 74078, USA

S. A. Trugman
Theoretical Division and Center for Integrated Nanotechnologies, Los Alamos National Laboratory, Los Alamos, New Mexico 87545, USA

(Received 15 December 2011; published 8 March 2012)

We apply a rigorous eigenmode analysis to study the electromagnetic properties of linear and weakly nonlinear metamaterials. The nonlinear response can be totally described by the linear eigenmodes when weak nonlinearities are attributed to metamaterials. We use this theory to interpret intrinsic second-harmonic spectroscopy on metallic metamaterials. Our study indicates that metamaterial eigenmodes play a critical role in optimizing a nonlinear metamaterial response to the extent that a poorly optimized modal pattern overwhelms the widely recognized benefits of plasmonic resonant field enhancements.

DOI: 10.1103/PhysRevB.85.125107 PACS number(s): 81.05.Xj, 42.65.−k

I. INTRODUCTION

Metamaterials are artificial composite materials engineered on a subwavelength scale to enable an optimized combination of electromagnetic (EM) properties that may not be readily available in nature (see Ref. 1 and the references cited therein). Metamaterials are often comprised of periodic arrays of "meta-atoms," subwavelength-sized resonators, that permit multiple theoretical descriptions of their EM properties. The small size and close packing of the resonators permits a macroscopic description where the metamaterial is approximated as a homogeneous medium with effective constitutive parameters such as permittivity or permeability.[2,3] Another possible method to analyze metamaterials is multipole analysis, a microscopic description in which scattered fields from an individual meta-atom are expressed as an expansion of multipole contributions.[4–7] When the meta-atom is thus described, as a collection of electric dipoles, magnetic dipoles, and electric quadrupoles for example, then the macroscopic or effective properties of the metamaterial may also be determined.

Still another description is frequently employed in metamaterial research. That is eigenmode (or modal) analysis. Eigenmodes are the meta-atom's spatial patterns of current, charge, and/or near-fields associated with metamaterial resonances. Eigenmodes are revealed during numerical simulations and are frequently used to visualize and interpret experimental measurements. Detailed knowledge of the eigenmodes provides a description of the EM response at both the microscopic and macroscopic levels, with more generality than multipolar analysis. There are various methods for determining EM eigenmodes and accessing the information they provide. Rigorous analytic methods exist for finding the eigenmodes of the simplest meta-atoms, such as cylinders and spheres.[8,9] Point group theoretical analysis, borrowed from molecular symmetry studies in spectroscopy, can reveal the character and existence of eigenmodes based on meta-atom symmetries.[10] Most often, meta-atom complexity requires that eigenmodes, particularly higher-order modes, be determined by numerical EM simulations. These provide the most detailed information at the usual cost of computational burden.

The utility of modal analysis has been revealed in research on coherent coupling between neighboring meta-atoms.[4,11–16] In these cases, as meta-atoms become closely spaced, their individual responses experience coupling through either shared electric or magnetic flux, or both. In a multipole expansion, the coupled pair could be treated as a single structure, and this should provide the correct far-field scattering. However, eigenmode analysis of the isolated meta-atoms quantifies the exact positions and orientations of polarized charge and circulating currents within the resonating structures. With this information it is relatively easy to qualitatively predict both the sign and onset of mutual coupling as the meta-atoms become closely spaced. This information is useful in explaining phenomena such as resonance splitting and frequency shifting.[11,12,15] Thoroughly understanding the metamaterial analog to electromagnetically induced transparency[17–22] is a similar eigenmode problem, particularly in determining the energy transfer between so-called bright, or radiative, and dark, or nonradiative, modes,[13,14] the latter of which have no dipole moment overlap with the externally exciting plane waves but are eigenmodes of the meta-atom nonetheless. Generally, coupled resonators and specially shaped asymmetric resonators enable narrow resonance linewidths, stronger dispersion, and stronger plasmonic field enhancements. This is particularly beneficial for linear metamaterial sensing applications,[23–26] and eigenmode analysis is critical to optimization in all such regards. Finally, recent work in nonlinear metamaterials is revealing yet another reason for detailed eigenmode analysis: to properly predict and understand observed nonlinear effects such as second harmonic generation (SHG).[27–31]

In this paper, we apply a rigorous eigenmode analysis to study both linear and nonlinear EM properties of metamaterials. More importantly, we point out that when weak nonlinearities are attributed to metamaterials, the nonlinear response can be totally described by the linear eigenmodes. This theory is further used to interpret intrinsic second-harmonic

spectroscopy on metallic metamaterials. Our study suggests that an enhanced nonlinear response requires optimization of both the resonance frequency and the modal pattern.

II. MODAL ANALYSIS FOR LINEAR METAMATERIALS

A. General description of the problem

Our initial goal is to find the eigenmodes and corresponding eigenfrequencies of a metamaterial comprised of periodically patterned metallic structures fabricated on top of a planar homogeneous substrate. It is assumed that the substrate has a permittivity $\epsilon_s(\omega)$ and is modeled as a semispace located at $z < 0$. The remaining $z > 0$ space is occupied by a homogeneous medium, which we will take as vacuum. For convenience, we assume the whole system is nonmagnetic, $\mu(\mathbf{r},\omega) = 1$.

In order to write Maxwell equations as an eigenvalue problem, we will assume that the permittivities of the substrate and metallic parts can be written as

$$\epsilon(\mathbf{r},\omega) = \epsilon_\infty(\mathbf{r})\left[1 - \frac{\omega_p^2(\mathbf{r})}{\omega^2 - \omega_0^2(\mathbf{r}) + i\omega\gamma(\mathbf{r})}\right], \tag{1}$$

where $\epsilon_\infty(\mathbf{r})$, $\omega_0(\mathbf{r})$, $\omega_p(\mathbf{r})$, and $\gamma(\mathbf{r})$ are constant within each region. Namely, the permittivity of the metal is described by a Drude model so that $\epsilon_\infty(\mathbf{r}) = 1$, $\omega_0(\mathbf{r}) = 0$ (effect of bound electrons is neglected), $\omega_p(\mathbf{r}) = \omega_p$ is the metal plasma frequency, and $\gamma(\mathbf{r}) = \gamma$ is the metal relaxation frequency. Within the (dielectric) substrate, $\epsilon_\infty(\mathbf{r}) = \epsilon_\infty$ is the high-frequency permittivity of the dielectric, $\omega_0(\mathbf{r}) = \omega_r$ is the (main) resonant frequency of the dielectric, and $\omega_p(\mathbf{r}) = \omega_{\rm osc}$ and $\gamma(\mathbf{r}) = \gamma_{\rm osc}$ are the oscillator strength and oscillator dissipation coefficient, respectively. Finally, for the vacuum, we have $\epsilon_\infty(\mathbf{r}) = 1$ and $\omega_p(\mathbf{r}) = 0$. It should be noticed that our method can be easily extended to incorporate permittivities with additional Lorentzian terms in Eq. (1), which in general are enough to model experimentally measured permittivities of the constituents of a metamaterial.

In each region, we can define the electric displacement $\mathbf{D}(\omega) = \epsilon_0\epsilon(\omega)\mathbf{E}(\omega) = \epsilon_0\epsilon_\infty\mathbf{E}(\omega) + \mathbf{P}(\omega)$, so that the polarization is given by $(\omega_0^2 - \omega^2 - i\omega\gamma)\mathbf{P}(\omega) = \epsilon_0\epsilon_\infty\omega_p^2\mathbf{E}(\omega)$. Further introducing the polarization current $\mathbf{J}(\omega) = -i\omega\mathbf{P}(\omega)$, the set of Maxwell equations can be reformulated as[32]

$$\omega\begin{pmatrix}\mathbf{H}\\ \mathbf{E}\\ \mathbf{P}\\ \mathbf{J}\end{pmatrix} = \begin{pmatrix} 0 & \frac{-i}{\mu_0}\nabla\times & 0 & 0\\ \frac{i}{\epsilon_0\epsilon_\infty(\mathbf{r})}\nabla\times & 0 & 0 & \frac{-i}{\epsilon_0\epsilon_\infty(\mathbf{r})}\\ 0 & 0 & 0 & i\\ 0 & i\epsilon_0\epsilon_\infty(\mathbf{r})\omega_p^2(\mathbf{r}) & -i\omega_0^2(\mathbf{r}) & -i\gamma(\mathbf{r})\end{pmatrix}\begin{pmatrix}\mathbf{H}\\ \mathbf{E}\\ \mathbf{P}\\ \mathbf{J}\end{pmatrix}. \tag{2}$$

This now has the form of an eigenvalue equation:

$$\omega\mathbf{u} = \mathcal{L}\mathbf{u}, \tag{3}$$

where $\mathbf{u} = (\mathbf{H},\mathbf{E},\mathbf{P},\mathbf{J})^{\rm T}$, and $\mathcal{L}$ is a non-Hermitian differential operator. As a consequence, the eigenvalues are in general complex, and the corresponding eigenvectors are not orthogonal to each other.[33,34] However, the eigenvectors are *biorthogonal* to the eigenvectors of the corresponding adjoint equation,

$$\lambda\mathbf{u}^\dagger = \mathbf{u}^\dagger\mathcal{L}^\dagger. \tag{4}$$

From the theory of non-self-adjoint differential equations, one knows that the eigenvalues and eigenvectors of the two mutually adjoint equations can be ordered in such a way that $\lambda_m = \omega_m^*$, and $\langle\mathbf{u}_m^\dagger|\mathbf{u}_{m'}\rangle = \delta_{m,m'}$ (here $\langle\ldots\rangle \equiv \int d^3\mathbf{r}\ldots$). Also, it is possible to associate the same eigenvalue ω_m with one eigenvector of Eq. (3) and with one eigenvector of the adjoint Eq. (4), i.e., $\omega_m \leftrightarrow \mathbf{u}_m,\mathbf{u}_m^{\dagger *}$. In the literature, $\mathbf{u}_m$ and $\mathbf{u}_m^{\dagger *}$ are generally called right and left eigenvectors, respectively.

The set of eigenvalues and eigenvectors contain very rich physics and highly useful information. In order to get some physical insight, let us consider first the following simple case. Assume a bandwidth of frequencies where both the metal and the substrate possess negligible dissipation, i.e., $\gamma(\mathbf{r}) = 0$ everywhere. In this case $\mathcal{L}$ is Hermitian, the eigenvalues are real, and the eigenvectors form a complete and orthogonal basis.[32] Let us further assume that the substrate is approximately dispersionless in this frequency bandwidth considered. Then, Maxwell equations can be written as a wave equation for the electric field as

$$\nabla\times\nabla\times\mathbf{E} + \frac{\omega_p^2}{c^2}f(\mathbf{r})\mathbf{E} = \frac{\omega^2}{c^2}\epsilon_{\rm out}(\mathbf{r})\mathbf{E}, \tag{5}$$

where $f(\mathbf{r})$ describes the geometry of the metamaterial [$f(\mathbf{r}) = 1$ for $\mathbf{r}$ belonging to the metamaterial structure and zero otherwise], and $\epsilon_{\rm out}(\mathbf{r}) = 1 + (\epsilon_s - 1)\theta(-z)$ with $\theta(z)$ being the Heaviside step function. This is an eigenvalue equation of the form $\mathcal{O}_1\mathbf{E} = \omega^2\mathcal{O}_2\mathbf{E}$, with $\mathcal{O}_{1,2}$ being self-adjoint operators. As is well known, variational expressions for eigenvalue problems can be found, both for dissipative and nondissipative systems. In the dissipationless case at hand, the variational expression for the eigenvalue is[35]

$$\omega^2 = \frac{\langle\mathbf{E}|\mathcal{O}_1\mathbf{E}\rangle}{\langle\mathbf{E}|\mathcal{O}_2\mathbf{E}\rangle}. \tag{6}$$

Equivalently

$$\omega^2 = \frac{\int d^3\mathbf{r}\left[|c\nabla\times\mathbf{E}|^2 + \omega_p^2 f(\mathbf{r})|\mathbf{E}|^2\right]}{\int d^3\mathbf{r}\epsilon_{\rm out}(\mathbf{r})|\mathbf{E}|^2}. \tag{7}$$

This equation relates the eigenvalues with the corresponding electric field eigenvector. One way to actually find both of them independently within this variational method is to find the stationary points of the r.h.s. of Eq. (7). Indeed, stationary points correspond to the eigenvalues, and the electric fields

at the minima correspond to the eigenfunctions. Since the stationary value for ω^2 is the corresponding eigenvalue, the electric field of a mode should be distributed around the metamaterial in such a way to minimize the numerator when $\epsilon_{\text{out}}(\mathbf{r})$ is positive and nearly constant. This observation is consistent with what was found in dielectric photonic crystals: The strongest electric flux is found in the high-ϵ regions associated with the lowest-frequency eigenmode.[36] This is also frequently observed in planar metamaterial experiments; a high-dielectric substrate reduces the resonance frequencies and encompasses most of the electric flux.[23]

Generally, the eigenvalue problem must be solved numerically and several approaches can be employed, including variational methods, finite-element methods, finite-different frequency-domain methods, and finite-difference time-domain methods (FDTD).[37,38] In the Appendix we briefly describe the FDTD method used in this paper.

It should be mentioned that, although the modal method is described above in the context of metamaterials, one can directly apply it to isolated or clustered nanoparticles. Furthermore, when the characteristic sizes of these are much smaller than the EM wavelength, our method can be simplified by using a quasistatic approximation.[39–41] More specifically, the spectral Bergman-Milton theory states that these electrostatic eigenmodes depend exclusively on the geometry of the nanoparticle, and the eigenmodes as well as the corresponding eigenvalues of two-dimensional particles are invariant under any conformal transformation.[42] These electrostatic eigenmodes can also be applied to study weak nonlinear or even quantum effects of plasmonic particles.[43]

B. Applications

When the metamaterial is illuminated by an external EM field, Maxwell equations can be written as

$$\omega \mathbf{U} = \mathcal{L}\mathbf{U} + \mathbf{S}, \tag{8}$$

where $\mathbf{S} = (0,0,0,\mathbf{J}_{\text{ext}})^{\text{T}}$ and $\mathbf{J}_{\text{ext}}(\mathbf{r},\omega)$ represents external current sources. The total field $\mathbf{U}$ can now be expanded in terms of the eigenvectors $\mathbf{u}_m$ of the source-free problem, namely

$$\mathbf{U}(\mathbf{r},\omega) = \sum_m \frac{\langle \mathbf{u}_m^\dagger | \mathbf{S} \rangle}{\omega - \omega_m} \mathbf{u}_m(\mathbf{r}), \tag{9}$$

where $\omega_m = \omega'_m + i\omega''_m$ are the corresponding complex eigenvalues of the source-free problem. A further simplification occurs when the incident field excites only one single mode, say the n-th mode; we then have

$$\mathbf{U}(\mathbf{r},\omega) \approx \frac{\langle \mathbf{u}_n^\dagger | \mathbf{S} \rangle}{\omega - \omega_n} \mathbf{u}_n(\mathbf{r}). \tag{10}$$

The overlap $\langle \mathbf{u}_n^\dagger | \mathbf{S} \rangle$ in the above equation quantitatively determines how strongly a general excitation will couple energy into or out of the single mode of interest. This concept may be visualized by considering the fundamental eigenmode of a split-ring resonator, shown in Fig. 1(a) as a map of the in-plane scalar electric potential. Parenthetically, the strongly dipolar nature of this mode illustrates why multipolar analysis can be an effective modeling tool. If the source is a normally-incident plane wave polarized in the y or z direction, $\mathbf{S}$ is

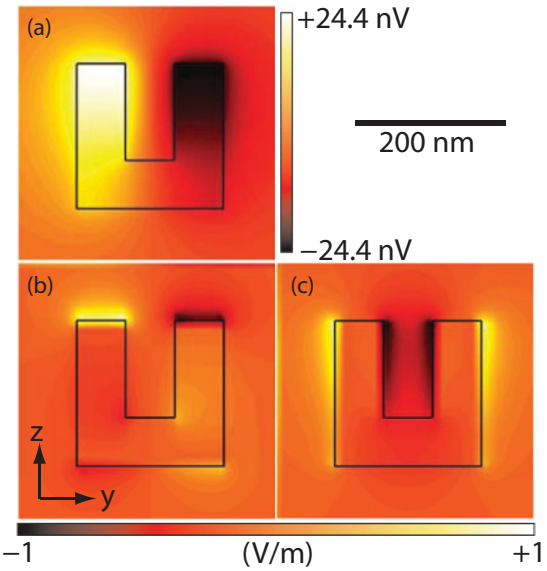

FIG. 1. (Color online) (a) In-plane scalar electric potential map of the fundamental eigenmode of a 25 nm thick gold split ring resonator (SRR) with dimensions indicated by the black scale bar to the right. Amplitude of in-plane (b) z- and (c) y-components of the electric field. Lower colorscale applies to (b) and (c). Though not visually obvious in (c) the y-directed fields within the gap region contribute more than those outside the SRR, leading to $\langle \mathbf{u}^\dagger | \mathbf{S} \rangle \neq 0$ in the overlap integral. For the particular eigenmode scaling in (c), this means regions where $E_y < 0$ cumulatively contribute more than regions where $E_y > 0$.

uniform and $\langle \mathbf{u}_1^\dagger | \mathbf{S} \rangle \propto \int dy\, dz\, (\mathbf{u}_1^{E\dagger} \cdot \hat{\mathbf{y}})$ or $\propto \int dy\, dz\, (\mathbf{u}_1^{E\dagger} \cdot \hat{\mathbf{z}})$, respectively. Here $\mathbf{u}^E$ stands for the electric field part of the eigenmode $\mathbf{u}$. The in-plane electric fields, calculated from the scalar potential, produce an approximate picture of these integrands and are shown in Figs. 1(b) and 1(c). The figures are a visual indication that $\langle \mathbf{u}_1^\dagger | \mathbf{S} \rangle \neq 0$ for y-polarized waves, and $\langle \mathbf{u}_1^\dagger | \mathbf{S} \rangle = 0$ for z-polarized waves. This knowledge is useful in certain applications, such as metamaterial sensing, for example. Modes with $\langle \mathbf{u}_n^\dagger | \mathbf{S} \rangle \to 0$ should have relatively long decay lifetimes, governed only by dissipative losses. The resulting narrow frequency response could make such modes more sensitive to small changes to its local dielectric environment. Obviously, all $\mathbf{u}_n^\dagger$ and $\mathbf{S}$ must be considered to properly utilize this approach.

Equation (10) is also applicable for calculating weak coupling between neighboring meta-atoms, where $\mathbf{S}$ consists of the near-fields of the neighbors. This information is required to determine, for example, resonance shifting effects of arrayed meta-atoms with different periodicities. In strongly coupled meta-atoms, the eigenmodes themselves are altered, leading to effects such as resonance splitting[11,12,15] and the metamaterial analog to electromagnetically induced transparency.[17–20] However, strongly-coupled meta-atoms may be analyzed as a single structure to yield a new set of eigenmodes. Equation (9) would be suitable for determining the response from such structures having eigenmodes that overlap in frequency.

Equation (10) can also be used to find the multipoles of one individual meta-atom directly.[4–6] When the characteristic size of the meta-atom is much smaller than the resonant

wavelength $\lambda_n = 2\pi c/\omega_n'$, we can describe the meta-atom in a multipole expansion, e.g., electric or magnetic dipoles. Taking the electric dipole as an example, the electric dipole polarizability tensor $\overleftrightarrow{\alpha}$ is given by

$$\overleftrightarrow{\alpha} \cdot \mathbf{E}_{\text{ext}} \approx \frac{\langle \mathbf{u}_n^\dagger | \mathbf{S} \rangle}{\omega - \omega_n} \int_{\text{meta-atom}} \mathbf{u}_n^P(\mathbf{r}) d^3\mathbf{r}, \tag{11}$$

where $\mathbf{E}_{\text{ext}}$ is the external electric field, $\mathbf{u}_n^P$ is the polarization part of the eigenvector $\mathbf{u}_n$ [the third component of the eigenvector in Eq. (2)], and the integration is performed over the meta-atom. We can further use the above equation to find the effective medium parameters (permittivity and permeability) of a metamaterial membrane formed by these meta-atoms. For example, let us consider a metamaterial that consists of an array of such meta-atoms located at positions $\mathbf{R}_n$, which is illuminated by a y-polarized external electric field propagating along the x direction (normal incidence), see Fig. 2. We also assume that $\overleftrightarrow{\alpha} = \text{diag}(\alpha_{xx}, \alpha_{yy}, \alpha_{zz})$. By approximating each of the meta-atoms as an ideal electric dipole, the resulting far-field zero-order reflection coefficient of the metamaterial is given by[44]

$$r = \frac{i\omega\mu_0 c/2A}{1/\alpha_{yy} - G_{yy}(0)}. \tag{12}$$

Here A is the area of the lattice unit cell, and

$$G_{yy}(0) = \sum_{n \neq 0} \mathcal{G}_{yy}^0(\mathbf{R}_n) \tag{13}$$

represents the collectively scattered fields at a given dipole at position $\mathbf{R}_{n=0}$ by the other dipoles at positions $\mathbf{R}_{n\neq 0}$ in the array ($\overleftrightarrow{\mathcal{G}}^0$ being the free-space Green function). The zero-order transmission coefficient is further given by $t = 1 + r$. Once we know the reflected and transmitted coefficients, the effective permittivity and permeability of the metamaterial can be extracted by treating the metamaterial membrane as a homogeneous slab with identical thickness.[3] Since the dipole polarizability of one single meta-atom varies rapidly around one resonance, we expect that the effective parameters of the corresponding metamaterial possess similar frequency dependence. One example is shown in Fig. 2, where the transmission spectrum of an array of gold cuboids is studied numerically and analytically, and reasonable agreement is observed.

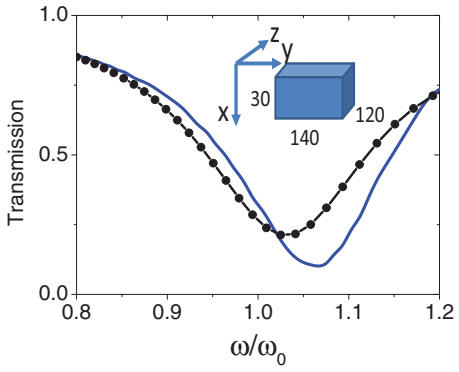

FIG. 2. (Color online) Transmission spectra of a 2D array of cuboids in a square lattice. The incident plane wave is y-polarized and propagates along the x direction (normal incidence). The dimensions of each cuboid are shown in the inset (all in nanometers), and the lattice constant is 320 nm. The corresponding polarizability of an isolated cuboid $\alpha_{yy} = 4\pi\epsilon_0 f/(\omega_0^2 - \omega^2 - i\omega\tau)$ with $\lambda_0 = 656$ nm, $f/\omega_0 = 6.5 \times 10^{-7}$ and $\tau/\omega_0 = 0.21$. The results obtained from the analytical discrete-dipole approximations (solid) agree reasonably well with those obtained from full numerical simulations (dotted).

III. WEAK NONLINEARITIES OF METAMATERIALS

While the linear applications of eigenmode analysis are familiar in the literature, there remains much to explore in the nonlinear realm. Nonlinear effects in metamaterials produce rich phenomena such as wave mixing and field modulation, that need to be understood at the microscopic level. When the nonlinearity is weak, the polarization $\mathbf{P}$ can be expanded in a power series of the electric field, as is usually done in nonlinear optics[45]

$$\mathbf{P}(\mathbf{r},t)/\epsilon_0 = \overleftrightarrow{\chi}^{(1)} \mathbf{E}(\mathbf{r},t) + \overleftrightarrow{\chi}^{(2)} \mathbf{E}(\mathbf{r},t) \cdot \mathbf{E}(\mathbf{r},t) + \ldots, \tag{14}$$

where $\overleftrightarrow{\chi}^{(1)}$ is the linear susceptibility tensor, $\overleftrightarrow{\chi}^{(2)}$ is the second-order nonlinear susceptibility tensor, etc. One can solve Maxwell equations perturbatively by also expanding the EM fields and currents to different orders in the nonlinearities, e.g. $\mathbf{E}(\mathbf{r},t) = \sum_n \mathbf{E}^{(n)}(\mathbf{r},t)$.[46] For example, for higher-order harmonic generation the different orders can be generally expressed as

$$\omega \mathbf{U}^{(n)} = \mathcal{L}\mathbf{U}^{(n)} + \mathbf{S}^{(n)}. \tag{15}$$

Note that without the source term $\mathbf{S}^{(n)}$ the above equation is identical to the general eigenvalue equation for the linear case (3). In other words, within perturbation theory nonlinear fields share the same set of eigenmodes as the linear fields. Consequently, the n-th order nonlinear field can be expanded in terms of these eigenvectors

$$\mathbf{U}^{(n)}(\mathbf{r},\omega) = \sum_m \frac{\langle \mathbf{u}_m^\dagger | \mathbf{S}^{(n)} \rangle}{\omega - \omega_m} \mathbf{u}_m(\mathbf{r}). \tag{16}$$

More importantly, since the nonlinear source $\mathbf{S}^{(n)}$ can usually be expressed as a function of lower order fields, for example $\overleftrightarrow{\chi}^{(n)} (\mathbf{E}^{(1)})^n$, we can calculate them recursively by using these eigenvectors exclusively.[47] This method can be very efficient under certain circumstances. Like its linear counterpart Eq. (10), Eq. (16) is especially useful when only one mode dominates and its position dependence and frequency dependence can be totally separated.

As an example, let us consider a tiny particle, such as a metallic nanoparticle, embedded within a much larger dipole antenna that is illuminated by an EM wave with frequency ω. We assume that the linear permittivity of the particle is close to that of the surrounding medium, so that it does not alter the eigenmodes of the antenna. It is further assumed that the particle possesses a third-order susceptibility $\overleftrightarrow{\chi}^{(3)}$, and that one of the antenna eigenmodes $\mathbf{u}_n$ has an eigenfrequency

$\omega_n = \omega_n' + i\omega_n''$ whose real part is almost equal to 3ω. The resulting third-harmonic field is given by

$$\mathbf{U}^{(3)}(\mathbf{r},3\omega) \approx \frac{i}{\omega_n''}\langle \mathbf{u}_n^{\dagger}(\mathbf{r})|\mathbf{S}^{(3)}(\mathbf{r})\delta(\mathbf{r}-\mathbf{r}_0)\rangle \mathbf{u}_n(\mathbf{r}), \tag{17}$$

where $\mathbf{r}_0$ is the location of the nonlinear particle. The above equation suggests that the spatial dependence of the third-harmonic signal is totally described by the eigenmode of the antenna. Note that the nonlinear source $\mathbf{S}^{(3)}(\mathbf{r})$ contains the information of the fundamental field $\mathbf{U}^{(1)}$. If we assume that $\mathbf{U}^{(1)}$ does not depend substantially on $\mathbf{r}$, then $\mathbf{S}^{(3)}$ is not sensitive to the location of the particle. Hence

$$\mathbf{U}^{(3)}(\mathbf{r},3\omega) \propto [\mathbf{u}_n^{\dagger}(\mathbf{r}_0)^* \cdot \mathbf{S}^{(3)}]\mathbf{u}_n(\mathbf{r}). \tag{18}$$

Therefore, similarly to the Purcell effect,[48] maximal third-harmonic intensity can be achieved by putting the nonlinear particle at the position of maximum local field enhancement in the 3ω eigenmode.

It should be mentioned that in the microwave region, lumped nonlinear insertions such as diodes are employed to achieve nonlinear metamaterials.[30,31,49] For example, tunable transmission and harmonic generation were observed in varactor-diode-based metamaterials.[31] As long as the nonlinearity is weak, the modal analysis method developed here is general enough to describe these nonlinear metamaterials as well. One challenge in this case is properly describing the electromagnetic behavior of the nonlinear insertion in terms of full-vector electric and magnetic fields, instead of the circuit quantities by which they are typically specified, such as scalar current and voltage. Fortunately, there are multiple methods to address or work around this challenge, some of which are already published.[37]

IV. FREQUENCY-DEPENDENCY OF INTRINSIC SHG IN METALLIC METAMATERIALS

We now use the above theory to study SHG in metamaterials. Recently several experimental and theoretical efforts have been carried out in this field.[27,50–57] One of the latest experiments is reported in Ref. 58, where SHG spectroscopy on 2D arrays of gold split-ring resonators (SRR) was studied. It was found that when the frequency of the incident EM field is close to the fundamental plasmonic resonance of the metamaterial, the frequency dependence of the SHG signal can be nearly described by a Lorentzian shaped curve. Surprisingly, illumination at the eigenfrequency of the fundamental plasmonic mode does not result in the maximal SH signal, even though this mode provides strong local field enhancement.

In the following we explain these observations by applying our modal approach to a structure similar to that of Ref. 58. We consider an array of gold SRRs arranged in a square lattice in the yz plane (one unit cell is depicted in the inset of Fig. 3). The incident plane wave is y-polarized and propagates along the x direction (normal incidence). Furthermore, both the fundamental and the SH wavelengths are much bigger than the lattice constant, so that no diffracted waves are allowed in the far zone. Consequently, only the eigenvectors with zero Bloch wave vector contribute to the linear and nonlinear fields. Moreover, because the structure possesses a $y = 0$ mirror symmetry, the eigenmodes can be divided into two groups

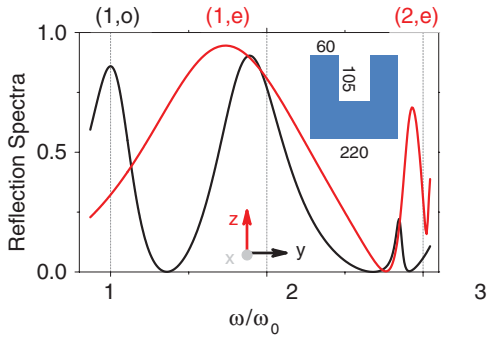

FIG. 3. (Color online) Reflection spectra of a 2D split-ring-resonator array with lattice constant of 305 nm. The incident plane wave propagates along the x direction and may be y-polarized (black) or z-polarized (red). The first-order odd mode (1,o) can be excited by the y-polarized incident field, and the first and second even modes, (1,e) and (2,e), can be excited by the z-polarized incident field. The inset shows a unit cell of the 2D array and its corresponding geometrical dimensions (the thickness of the SRR is 25 nm). All the dimensions are in nanometers.

in terms of the z component of the electric field. It can be even such that

$$E_z(x,y,z) = E_z(x,-y,z),\ E_y(x,y,z) = -E_y(x,-y,z),$$

or be odd so that

$$E_z(x,y,z) = -E_z(x,-y,z),\ E_y(x,y,z) = E_y(x,-y,z).$$

Note that E_x shares the same symmetry properties as E_z. To simplify our notation, we use $\omega_{n,i}$ and $\mathbf{u}_{n,i}$, with $i = o,e$, to denote these eigenvalues as well as eigenvectors. Moreover, we have the following orthogonal relations

$$\langle \mathbf{u}_{n',i}^{\dagger}|\mathbf{u}_{n',i'}\rangle = \delta_{n,n'}\delta_{i,i'}, \tag{19}$$

i.e., two eigenvectors with different symmetry are orthogonal.

For simplicity, we assume that the gold permittivity is described by a Drude model, Eq. (1), with plasma frequency $\omega_p = 1.367 \times 10^{16}\mathrm{s}^{-1}$ and the phenomenological collision frequency $\gamma = 6.478 \times 10^{13}\mathrm{s}^{-1}$.[46] Using the FDTD method, the linear spectra of the free-standing SRR array is calculated and the results are plotted in Fig. 3. Notice that the y-polarized incident EM field (solid black line) excites the odd eigenmodes exclusively, while the even eigenmodes can only be excited by z-polarized illumination. The real part of the eigenvalues can be identified from the peaks of the reflection spectra (see the Appendix), while the imaginary part can be obtained by fitting the spectra with a Lorentzian form (see below). We find that the fundamental odd mode has a resonant frequency of $\omega_{1,o} = (1 + 0.173i)\omega_0$, with $\omega_0 = 1.547 \times 10^{15}\mathrm{s}^{-1}$, and the two lowest-order even eigenmodes have eigenvalues $\omega_{1,e} = (1.74 + 0.644i)\omega_0$ and $\omega_{2,e} = (2.93 + 0.069i)\omega_0$, respectively. Note that the (2,e) mode has a damping loss much smaller than that of the (1,e) mode, a phenomenon that has been observed numerically in Ref. 59.

As in Ref. 58 we choose the incident frequency quite close to ω_0. Consequently only the lowest-order odd mode contributes significantly to the linear fields, i.e.,

$$\mathbf{U}^{(1)}(\omega,\mathbf{r}) \approx \frac{\langle \mathbf{u}_{1,o}^{\dagger}|\mathbf{S}^{(1)}\rangle}{\omega-\omega_{1,o}}\mathbf{u}_{1,o}(\mathbf{r}). \tag{20}$$

Because of the structural symmetry, only z-polarized SH far-field signals are allowed. In other words, only the even eigenmodes contribute to the second-order fields

$$\mathbf{U}^{(2)}(2\omega,\mathbf{r}) = \sum_m \frac{\langle \mathbf{u}_{m,e}^{\dagger}|\mathbf{S}^{(2)}\rangle}{2\omega-\omega_{m,e}}\mathbf{u}_{m,e}(\mathbf{r}). \tag{21}$$

Within perturbation theory the nonlinear source $\mathbf{S}^{(2)}$ can be connected with the linear field $\mathbf{U}^{(1)}$ as

$$\mathbf{S}^{(2)} = \mathcal{X}\mathbf{U}^{(1)}\mathbf{U}^{(1)} \approx \left[\frac{\langle \mathbf{u}_{1,o}^{\dagger}|\mathbf{S}^{(1)}\rangle}{\omega-\omega_{1,o}}\right]^2 \mathcal{X}\mathbf{u}_{1,o}\mathbf{u}_{1,o}, \tag{22}$$

where $\mathcal{X}$ is an operator whose form is determined by the particular form of the nonlinearity, and can encompass different nonlinear mechanisms presented in Refs. 46, 53, 57, and 60. For example, for the hydrodynamic model (see below) $\mathcal{X}$ is a differential operator given by the last three terms of Eq. (26).

Inserting the above equation in (21), we obtain the second-order field

$$\mathbf{U}^{(2)}(2\omega,\mathbf{r}) \approx \sum_m \frac{\alpha_{m,e}}{(2\omega-\omega_{m,e})(\omega-\omega_{1,o})^2}\mathbf{u}_{m,e}(\mathbf{r}), \tag{23}$$

where

$$\alpha_{m,e} = \langle \mathbf{u}_{1,o}^{\dagger}|\mathbf{S}^{(1)}\rangle^2 \langle \mathbf{u}_{m,e}^{\dagger}|\mathcal{X}\mathbf{u}_{1,o}\mathbf{u}_{1,o}\rangle. \tag{24}$$

It is interesting to notice that when only the (n,e) mode dominates $\mathbf{U}^{(2)}$, and $\alpha_{n,e}$ is frequency-independent, the frequency dependence of the SH intensity can be simply described by

$$\left|\frac{1}{(2\omega-\omega_{n,e})(\omega-\omega_{1,o})^2}\right|^2. \tag{25}$$

This expression will result in a Lorentzian shaped curve, similar to the experimental observations.[58,61] Additionally, for $\omega'_{n,e}/2 < \omega'_{1,o}$, the maximal SH intensity is generated when the fundamental illumination is red shifted from $\omega'_{1,o}$, and for $\omega'_{n,e}/2 > \omega'_{1,o}$, the maximum SH intensity is generated when the fundamental is blue shifted from $\omega'_{1,o}$. Furthermore, the damping losses of these two eigenmodes, especially the (1,o) mode, affect the peak location strongly. As an example, by choosing either the (1,e) and (2,e) as dominant, we can plot the resulting frequency dependence of the SH intensity, as shown in Fig. 4. These two modes give similar Lorentzian shaped curves, but the SH intensity as a function of illumination frequency peaks at different sides of ω_0.

To determine which even mode dominates the SH process, we must estimate the overlap coefficients $\alpha_{m,e}$, or more precisely the overlap between the even mode and the nonlinear source, i.e., $\langle \mathbf{u}_{m,e}^{\dagger}|\mathcal{X}\mathbf{u}_{1,o}\mathbf{u}_{1,o}\rangle$. This requires a full understanding of the SH mechanism.[46,53,57,60] Before discussing these results we note that there are general features of SHG from metallic nanostructures that indicate which

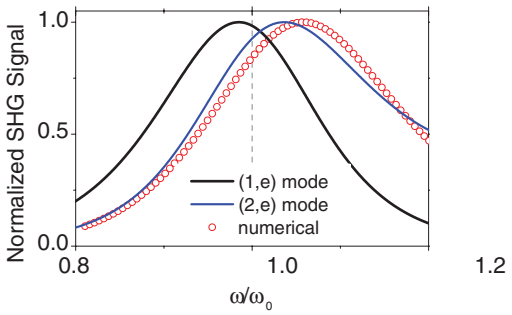

FIG. 4. (Color online) The frequency dependence of the SH intensity from the 2D SRR array of Fig. 3, as obtained from the single-mode approximation Eq. (25), as well as the results of a full-wave numerical simulation (dotted) based on the classical hydrodynamic model described by Eq. (26).

mode will dominate. Because of the centrosymmetry of metal, the electric dipole approximation suggests that the SH polarization is strongly localized near the metallic surfaces and corners.[45] This approximation is reasonable, as supported by experimental[55] as well as numerical observations.[54] An even mode with field enhanced near these hot spots should therefore lead to a strong overlap with the SH source. In Fig. 5 we plot the near field distributions of the (1,o) mode as well as the first two even modes. Notice that the (2,e) mode is strongly localized around the corners. [Our (2,e) mode pattern deviates considerably from the one in Ref. 59 mainly because our structure has a very wide metallic bottom.] Moreover, as suggested by Eq. (7) and confirmed by Fig. 5, the (2,e) mode has a higher degree of field enhancement inside the metal than the (1,e) mode. Therefore it is likely that the (1,e) mode does not dominate the second-order process, despite the fact that its frequency is very close to $2\omega'_{1,o}$.

To support the discussion above, we numerically calculate the SH spectroscopy of the SRR array by using the classical hydrodynamic model developed in Ref. 46. Within this model, charge transport inside the metal is described as a classical fluid characterized by the electron number density $n(\mathbf{r},t)$ and the electron velocity field $\mathbf{v}(\mathbf{r},t)$. The dynamics of this fluid under the influence of Lorentz forces in the presence of an external EM wave is self-consistently described by Maxwell equations coupled with the electronic current density $\mathbf{j}(\mathbf{r},t) = en(\mathbf{r},t)\mathbf{v}(\mathbf{r},t)$ (here e is the electron charge). The second-order current density satisfies[46]

$$\frac{\partial \mathbf{j}^{(2)}}{\partial t} = -\gamma \mathbf{j}^{(2)} + \frac{e^2 n_0}{m_e}\mathbf{E}^{(2)} + \sum_k \frac{\partial}{\partial r_k}\left(\frac{\mathbf{j}^{(1)} j_k^{(1)}}{en_0}\right) - \frac{e}{m_e}[\epsilon_0(\nabla\cdot\mathbf{E}^{(1)})\mathbf{E}^{(1)} + \mathbf{j}^{(1)}\times\mathbf{B}^{(1)}]. \tag{26}$$

Here n_0 is the background ionic density, m_e is the electron mass, the subscripts k denote Cartesian coordinates, and the term $-\gamma\mathbf{j}^{(2)}$ corresponds to current damping. Numerically it is found that the leading source of nonlinearity is the third term in Eq. (26).[51] This model was shown not only to provide qualitative agreement with experiments but also to reproduce the overall strength of the experimentally observed SH signals.[46]

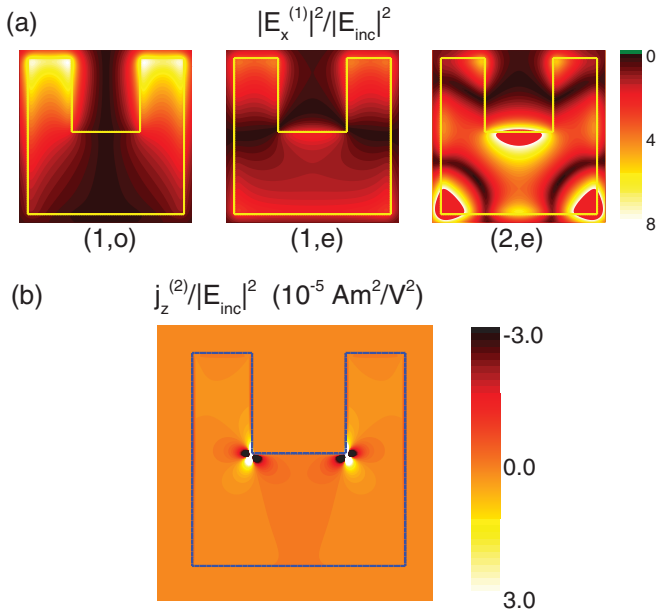

FIG. 5. (Color online) (a) Near field distributions of the three lowest eigenmodes for the 2D SRR array shown in Fig. 3. (b) The z component of the SH current is obtained by using the hydrodynamic model.

The numerical simulation for the SRR array of Fig. 3 is depicted as the dotted curve in Fig. 4. This is visually verified in Fig. 5 which shows that the calculated SH current exhibits a much stronger overlap with the (2,e) mode than with the (1,e) mode. Remarkably, the (1,e) mode shows pronounced nulls precisely where SH current is maximized, indicating a very poor ability to radiate SH signal. We find that our simulation reasonably agrees with the (2,e) mode approximation, implying that the (2,e) mode significantly contributes to the SH signal. We also considered two additional structures: an SRR array deposited on top of a semi-infinite glass substrate, and a free-standing array with slight asymmetry (by increasing one metallic arm width from 60 nm to 80 nm). In both these cases we obtained results similar to the ones in Fig. 4 (a symmetric free-standing SRR array). Specifically, for the first structure, the maximal SHG appears around $1.05\omega_0'$, with $\omega_0' = 1.25 \times 10^{15}\text{s}^{-1}$ being the frequency of the fundamental odd mode; for the second one, the maximal SHG appears around $1.06\omega_0'$, with $\omega_0' = 1.57 \times 10^{15}\text{s}^{-1}$. We conclude that the modal pattern affects SHG considerably, as suggested by Eq. (24). As in the linear case, this example shows that maximal SH radiation occurs when there is strong overlap between a meta-atom eigenmode and the source field. The key implication of our analysis is that, in order to achieve optimized nonlinear effects, one needs to pay attention not only to field enhancements but also to modal pattern. Whereas the field enhancement determines the strength of the nonlinear conversion, the modal pattern determines how well the nonlinear fields are radiated from the metamaterial.

We mention that the experimental observations in Ref. 58 are more similar to the (1,e) mode approximation in Fig. 4. In other words, the (1,e) mode dominates in the experimental SH signals. One possible origin of this discrepancy between the experiment and our simulation are imperfections in the experimental sample (such as fabrication distortions that cause meta-atoms to be nonidentical) that might impact the (2,e) mode more strongly. The loss in this mode becomes so great that its contribution to SHG is almost negligible. Interestingly, another similar experiment using a slightly different sample observed two peaks' SH signals on both sides of ω_0.[61]

V. CONCLUSIONS

In this work a rigorous eigenmode analysis is developed to study linear and nonlinear electromagnetic properties of metamaterials. The utility of eigenmode analysis is discussed for its ability to describe and visualize metamaterial behaviors such as scattering, inter-resonator coupling, and plasmonic field enhancement, all of which underpin metamaterial applications. A general mathematical description of the eigenmode problem is provided and quantitatively linked to recent theoretical and applied research topics such as multipolar analysis and metamaterial sensing. The formulation is then shown to apply equally well to weak nonlinear phenomena, reproducing the frequency dependence observed in SHG in metallic metamaterials, without regard to the form of the actual nonlinear mechanism. More importantly, using modal analysis and a classical hydrodynamic model of the nonlinear mechanism, it is established that the modal pattern can play an equal or greater role than plasmonic field enhancement in optimizing macroscopic nonlinear metamaterial behavior. In conclusion, this work visually and mathematically illustrates that the understanding and optimization of metamaterial eigenmodes is essential for improving metamaterial performance, particularly as multiple resonant frequencies become involved, as in recent nonlinear work.

ACKNOWLEDGMENTS

The authors wish to thank Weili Zhang for carefully reading this manuscript. We acknowledge support from the LANL LDRD program. This work was carried out under the auspices of the National Nuclear Security Administration of the US Department of Energy at Los Alamos National Laboratory under Contract No. DE-AC52-06NA25396.

APPENDIX: FINDING EIGENMODES USING THE FDTD METHOD

One popular approach to calculate eigenmodes is based on the FDTD method.[37] To interpret this approach, we start from Eq. (8),

$$\omega\mathbf{U} = \mathcal{L}\mathbf{U} + \mathbf{S},$$

with $\mathbf{S}$ representing specific external excitations.[37] Correspondingly, the adjoint equation is given by $\lambda\mathbf{U}^\dagger = \mathbf{U}^\dagger\mathcal{L}^\dagger + \mathbf{S}^\dagger$. Let us now split $\mathbf{U} = \mathbf{U}_{\text{ind}} + \mathbf{U}_0$, where $\mathbf{U}_0$ is the solution to $\omega\mathbf{U}_0 = \mathcal{L}_0\mathbf{U}_0 + \mathbf{S}$, where $\mathcal{L}_0$ is the operator for the case when the metamaterial is absent (i.e., only the vacuum-substrate interface is considered). By subtracting it from Eq. (8) we arrive at

$$\omega\mathbf{U}_{\text{ind}} - \mathcal{L}\mathbf{U}_{\text{ind}} = (\mathcal{L} - \mathcal{L}_0)\mathbf{U}_0. \quad \text{(A1)}$$

We now expand $\mathbf{U}_{\text{ind}}$ in terms of the source-free right-eigenvectors $\mathbf{u}_m$ of Eq. (3),

$$\mathbf{U}_{\text{ind}}(\mathbf{r},\omega) = \sum_m \alpha_m(\omega)\mathbf{u}_m(\mathbf{r}), \tag{A2}$$

where the expansion coefficients can be obtained by projecting onto the left eigenvectors $\alpha_m(\omega) = \langle \mathbf{u}_m^\dagger | \mathbf{U}_{\text{ind}} \rangle$. Substituting it into Eq. (A1) and further projecting onto the left eigenvectors, we obtain

$$\alpha_m(\omega) = \frac{1}{\omega - \omega_m} \langle \mathbf{u}_m^\dagger | (\mathcal{L} - \mathcal{L}_0) | \mathbf{U}_0 \rangle, \tag{A3}$$

where the complex frequency ω_m can be written in terms of its real and imaginary parts, namely $\omega_m = \omega'_m + i\omega''_m$. Assuming the inner product $\langle \mathbf{u}_m^\dagger | (\mathcal{L} - \mathcal{L}_0) | \mathbf{U}_0 \rangle$ is a nonzero, slowly-varying function of frequency around ω'_m, we can approximate $\mathbf{U}_{\text{ind}}(\mathbf{r},\omega)$ in a narrow region centered at ω'_m as

$$\mathbf{U}_{\text{ind}}(\mathbf{r},\omega) \approx \frac{1}{\omega - \omega_m} \langle \mathbf{u}_m^\dagger | (\mathcal{L} - \mathcal{L}_0) | \mathbf{U}_0 \rangle \ \mathbf{u}_m(\mathbf{r}). \tag{A4}$$

Consequently the frequency-dependency of $\mathbf{U}_{\text{ind}}$ in this region can be fitted by a Lorentz formula

$$\frac{\omega - \omega'_m + i\omega''_m}{(\omega - \omega'_m)^2 + \omega''^2_m}. \tag{A5}$$

More specifically, we know that

$$|\mathbf{U}_{\text{ind}}(\omega)|^2 \propto \frac{1}{(\omega - \omega'_m)^2 + \omega''^2_m}, \tag{A6}$$

resembles a Lorentzian shape. Its peak appears at ω'_m, and ω''_m can be obtained by using

$$\omega''_m = \frac{\Delta\omega}{\sqrt{|\frac{\mathbf{U}_i(\omega'_m)}{\mathbf{U}_i(\Delta\omega+\omega'_m)}|^2 - 1}}, \tag{A7}$$

where $\Delta\omega$ represents a tiny frequency shift from ω'_m. As a result, by fitting the frequency-dependency of $\mathbf{U}_{\text{ind}}$ with a Lorentz formula we can obtain the real and imaginary parts of the complex eigenvalue ω_m.

All of these considerations simply show that the complex eigenfrequencies can be obtained by doing a modal analysis in the frequency-domain and looking at the positions where the mode response is peaked in frequency. We now describe how to find the complex eigenfrequencies and eigenfunctions using the FDTD approach. In FDTD one assumes a few random currents, usually point sources with a $\delta(t - t_0)$ time dependency or narrow Gaussian pulses, located close to the metamaterial structure. The radiation of the current sources are supposed to excite all the eigenvectors of the system. The evolution of polarization currents $\mathbf{J}(\mathbf{r},t)$ at a few positions inside the structure are then recorded. Fourier transforming these signals, one obtains their frequency dependence $\mathbf{J}(\mathbf{r},\omega)$. The maxima of the current amplitude $|\mathbf{J}(\mathbf{r},\omega)|$ indicate the locations of the real parts of the eigenfrequencies, ω'_m. Then, ω''_m can be found by using Eq. (A7). Note that these eigenvalues do not depend on the excitations nor on the observation locations we chose. Once the complex eigenfrequencies are determined, the corresponding eigenvectors can be found by choosing a time-harmonic current source oscillating at ω'_m and finding the resulting eigenvector $\mathbf{u}_m$.

[1] L. Solymar and E. Shamonina, *Waves in Metamaterials* (Oxford University Press, Oxford, 2009).

[2] J. B. Pendry, A. J. Holden, D. J. Robbins, and W. J. Stewart, IEEE Trans. Microwave Theory Tech. **47**, 2075 (1999).

[3] D. R. Smith, S. Schultz, P. Markoš, and C. M. Soukoulis, Phys. Rev. B **65**, 195104 (2002).

[4] Y. Zeng, C. Dineen, and J. V. Moloney, Phys. Rev. B **81**, 075116 (2010).

[5] J. Petschulat, J. Yang, C. Menzel, C. Rockstuhl, A. Chipouline, P. Lalanne, A. Tüennermann, F. Lederer, and T. Pertsch, Opt. Express **18**, 14454 (2010).

[6] C. Rockstuhl, C. Menzel, S. Mühlig, J. Petschulat, C. Helgert, C. Etrich, A. Chipouline, T. Pertsch, and F. Lederer, Phys. Rev. B **83**, 245119 (2011).

[7] J. Petschulat, A. Chipouline, A. Tünnermann,T. Pertsch, C. Menzel, C. Rockstuhl, T. Paul, and F. Lederer, Phys. Rev. B **82**, 075102 (2010).

[8] J. A. Stratton, *Electromagnetic Theory* (McGraw-Hill, New York, 1941).

[9] R. E. Collin, *Field Theory of Guided Waves* (Wiley-Interscience-IEEE, New York, 1991).

[10] W. J. Padilla, Opt. Express **15**, 1639 (2007).

[11] I. Sersic, M. Frimmer, E. Verhagen, and A. F. Koenderink, Phys. Rev. Lett. **103**, 213902 (2009).

[12] M. T. Reiten, D. Roy Chowdhury, J. Zhou, A. J. Taylor, J. F. O'Hara, and A. K. Azad, Appl. Phys. Lett. **98**, 131105 (2011).

[13] S.-Y. Chiam, R. Singh, C. Rockstuhl, F. Lederer, W. Zhang, and A. A. Bettiol, Phys. Rev. B **80**, 153103 (2009).

[14] B. Kang, E. Choi, H.-H. Lee, E. S. Kim, J. H. Woo, J. Kim, T. Y. Hong, J. H. Kim, and J. W. Wu, Opt. Express **18**, 11552 (2010).

[15] D. Roy Chowdhury, R. Singh, M. Reiten, J. Zhou, A. J. Taylor, and J. F. O'Hara, Opt. Express **19**, 10679 (2011).

[16] D. A. Powell, M. Lapine, M. V. Gorkunov, I. V. Shadrivov, and Y. S. Kivshar, Phys. Rev. B **82**, 155128 (2010).

[17] N. Papasimakis, V. A. Fedotov, N. I. Zheludev, and S. L. Prosvirnin, Phys. Rev. Lett. **101**, 253903 (2008).

[18] P. Tassin, L. Zhang, Th. Koschny, E. N. Economou, and C. M. Soukoulis, Phys. Rev. Lett. **102**, 053901 (2009).

[19] Z.-G. Dong, H. Liu, J.-X. Cao, T. Li, S.-M. Wang, S.-N. Zhu, and X. Zhang, Appl. Phys. Lett. **97**, 114101 (2010).

[20] Z.-G. Dong, H. Liu, M.-X. Xu, T. Li, S.-M. Wang, J.-X. Cao, S.-N. Zhu, and X. Zhang, Opt. Express **18**, 22412 (2010).

[21] J. Kim, R. Soref, and W. R. Buchwald, Opt. Express **18**, 17997 (2010).

[22] V. T. T. Thuy, N. T. Tung, J. W. Park, V. D. Lam, Y. P. Lee, and J. Y. Ree, J. Opt. **12**, 115102 (2010).

[23] J. F. O'Hara, R. Singh, I. Brener, E. Smirnova, J. Han, A. J. Taylor, and W. Zhang, Opt. Express **16**, 1786 (2008).

[24]Z.-G. Dong, H. Liu, M.-X. Xu, W.-B. Lu, and S.-N. Zhu, Phys. Lett. A **375**, 1148 (2011).
[25]C. Debus and P. H. Bolivar, Appl. Phys. Lett. **91**, 184102 (2007).
[26]I. A. I. Al-Naib, C. Jansen, and M. Koch, Appl. Phys. Lett. **93**, 083507 (2008).
[27]M. W. Klein, C. Enkrich, M. Wegener, and S. Linden, Science **313**, 502 (2006).
[28]M. W. Klein, M. Wegener, N. Feth, and S. Linden, Opt. Express **15**, 5238 (2007).
[29]H. Husu, B. K. Canfield, J. Laukkanen, B. Bai, M. Kiuttinen, J. Turunen, and M. Kauranen, Metamaterials **2**, 155 (2008).
[30]M. Lapine, M. Gorkunov, and K. H. Ringhofer, Phys. Rev. E **67**, 065601(R) (2003).
[31]I. V. Shadrivov, A. B. Kozyrev, D. W. van der Weide, and Y. S. Kivshar, Appl. Phys. Lett. **93**, 161903 (2008).
[32]A similar equation for materials with a Lorentz-type permittivity was written by A. Raman and S. Fan, Phys. Rev. Lett. **104**, 087401 (2010).
[33]R. Cole, *Theory of Ordinary Differential Equations* (Appleton-Century-Crofts, New York, 1968).
[34]M. Naimark, *Linear Differential Operators, Part 1*, edited by W. Everitt (Ungar, New York, 1968).
[35]W. C. Chew, *Waves and Fields in Inhomogeneous Media* (IEEE Press, New York, 1995).
[36]J. D. Joannopoulos, S. G. Johnson, J. N. Winn, and R. D. Meade, *Photonic Crystals: Molding the Flow of Light*, 2nd Ed. (Princeton University Press, Princeton, 2008).
[37]A. Taflove and S. C. Hagness, *Computational Electrodynamics: The finite-difference time-domain method*, 2nd Ed. (Artech House, Boston, 2000).
[38]K. Yee, IEEE Trans. Antennas and Propagat. **14**, 302 (1996).
[39]D. J. Bergman and D. Stroud, in *Solid State Physics*, edited by H. Ehrenreich and D. Turnbull (Academic, Boston, 1992), Vol. 46, pp. 148–270.
[40]G. W. Milton, *The Theory of Composites* (Cambridge University Press, Cambridge, 2002).
[41]I. D. Mayergoyz, D. R. Fredkin, and Z. Zhang, Phys. Rev. B **72**, 155412 (2005).
[42]Y. Zeng, J. Liu, and D. Werner, Opt. Express **19**, 20035 (2011).
[43]M. I. Stockman, *Electromagnetic Theory of SERS* (Springer, New York, 2006).
[44]F. J. García de Abajo, Rev. Mod. Phys. **79**, 1267 (2007).
[45]R. W. Boyd, *Nonlinear Optics*, 2nd Ed. (Academic Press, New York, 2003).
[46]Y. Zeng, W. Hoyer, J. Liu, S. W. Koch, and J. V. Moloney, Phys. Rev. B **79**, 235109 (2009).
[47]W. Hoyer and S. W. Koch, private communication.
[48]E. M. Purcell, Phys. Rev. **69**, 681 (1946).
[49]J. F. O'Hara, M. T. Reiten, P. Colestock, L. Earley, and A. Taylor, Proc. SPIE **8093**, 809304 (2011).
[50]S. Kujala, B. K. Canfield, M. Kauranen, Y. Svirko, and J. Turunen, Phys. Rev. Lett. **98**, 167403 (2007).
[51]N. Feth, S. Linden, M. W. Klein, M. Decker, F. Niesler, Y. Zeng, W. Hoyer, J. Liu, S. W. Koch, J. V. Moloney, and M. Wegener, Opt. Lett. **33**, 1975 (2008).
[52]E. Kim, F. Wang, W. Wu, Z. Yu, and Y. R. Shen, Phys. Rev. B **78**, 113102 (2008).
[53]W. L. Schaich, Phys. Rev. B **78**, 195416 (2008).
[54]Y. Zeng and J. V. Moloney, Opt. Lett. **34**, 2844 (2009).
[55]V. K. Valev, A. V. Silhanek, N. Verellen, W. Gillijns, P. Van Dorpe, O. A. Aktsipetrov, G. A. E. Vandenbosch, V. V. Moshchalkov, and T. Verbiest, Phys. Rev. Lett. **104**, 127401 (2010).
[56]J. Butet, G. Bachelier, I. Russier-Antoine, C. Jonin, E. Benichou, and P.-F. Brevet, Phys. Rev. Lett. **105**, 077401 (2010).
[57]M. Scalora, M. A. Vincenti, D. de Ceglia, V. Roppo, M. Centini, N. Akozbek, and M. J. Bloemer, Phys. Rev. A **82**, 043828 (2010).
[58]F. B. P. Niesler, N. Feth, S. Linden, and M. Wegener, Opt. Lett. **36**, 1533 (2011).
[59]C. Rockstuhl, F. Lederer, C. Etrich, T. Zentgraf, J. Kuhl, and H. Giessen, Opt. Express **14**, 8827 (2006).
[60]J. I. Dadap, J. Shan, K. B. Eisenthal, and T. F. Heinz, Phys. Rev. Lett. **83**, 4045 (1999); V. L. Brudny, B. S. Mendoza, and W. L. Mochan, Phys. Rev. B **62**, 11152 (2000); W. L. Mochan, J. A. Maytorena, B. S. Mendoza, and V. L. Brudny, *ibid.* **68**, 085318 (2003).
[61]M. Gentile, M. Hentschel, R. Taubert, H. Guo, H. Giessen, and M. Fiebig, Appl. Phys. B **105**, 149 (2011).